Journal of Engineering Science and Technology
Vol. 16, No. 6 (2021) 4687 - 4706

EFFECT OF SLAG CEMENT ON CONCRETE RESISTANCE AGAINST COMBINED EXPOSURE TO FREEZE-THAW AND CHLORIDE INGRESS

JUN ZHAO[1], ESKINDER DESTA SHUMUYE[1,*], ZIKE WANG[2]

[1]School of Civil Engineering, Zhengzhou University, Zhengzhou 450001, China
[2]School of Mechanics and Safety Engineering, Zhengzhou University, Zhengzhou 450001, China
*Corresponding Author: eskdes@gmail.com

Abstract

In cold climates, de-icers such as sodium chloride (NaCl) and calcium chloride ($CaCl_2$), which pose a significant risk of chloride-induced corrosion of steel in concrete structure are often used to reduce the slipperiness of the pavement surface triggered by snowfall. Hence, minimizing severe durability deterioration of the existing concrete structure is essential to maintain serviceability of the concrete structure. The aim of this study is to investigate the durability of concrete produced by combining ordinary Portland cement (OPC) with ground-granulated blast-furnace slag (GGBS). Concrete specimens cast with OPC and various percentages of GGBS (0%, 30%, 50%, and 70%) were subjected to extensive experimental tests reproducing basic freeze-thaw cycles and a chloride-ion attack to determine their combined effects and the resultant concentrations of free water-soluble chloride ions within the concrete samples. The porosities and pore-size distributions were determined via mercury intrusion porosimetry (MIP). Furthermore, the chloride ion threshold levels and diffusion coefficients were analyzed using NELD-CL420 ion-selective electrodes and NELD-AL492 rapid chloride permeability test apparatus, respectively. The results demonstrate that the concrete specimens containing GGBS exhibited greater resistance to chloride ion penetration than the conventional concrete specimens. Further, this resistance increased with the increasing percentage of GGBS, and concrete specimens with higher percentages of GGBS exhibited greater resistance to the combined effects of chloride ion attack and freeze-thaw exposure. Finally, MIP results indicate that the porosities of the specimens decreased with increasing GGBS percentage and resulted in lower concentrations of water-soluble chloride ions.

Keywords: Chloride, Freeze-thaw, GGBS, Ion Selective Electrodes, MIP, Porosity, RCPT.

1. Introduction

Cement production is an energy-consuming process that has a significant impact on the environment; on average, the cement industry contributes approximately 8% of the annual global CO_2 emissions [1]. Further, the production of Portland cement releases approximately one metric ton of CO_2 into the surrounding atmosphere per one metric tons of cement produced [2, 3]. Due to the increasing rate of global warming, priority is being given to environmental regulations that mitigate ecological damage by encouraging the use of supplementary cementitious materials, such as ground-granulated blast-furnace slag (GGBS) and fly ash [3-5]. However, because concrete structures can be affected by frost and chemical attacks, the durability of concrete is a primary consideration in selecting the appropriate cementitious materials and thereby maximizing the lifespans of concrete structures. In particular, frost damage is one of the major factors affecting concrete durability in colder regions [6]. Concrete structures will deteriorate if permeated by water, and reinforced concrete is particularly susceptible to deterioration caused by chloride ions that penetrate the concrete and corrode the reinforcement bars. Another common durability issue in concrete structures is salt attack, which usually occurs in pavements due to exposure to de-icing salts. Additionally, the degradation of concrete due to chloride salts can be exacerbated by the action of freeze-thaw cycles.

Supplementary cementitious materials such as GGBS, silica fume, and fly ash are often utilized as partial substitutions for conventional cementitious materials in the production of concrete. These supplementary materials can fill voids inside porous concrete and therefore enhance pozzolanic reactions. Many researchers have suggested that GGBS cement exhibits superior resistance to chloride penetration [7, 8]. The chloride binding capacity of a cement matrix is a major factor in determining its resistance to chloride ion penetration [9], and the high resistance of GGBS cement is indicative of its effective binding characteristics. However, given that in ACI 233R-03, slag cement blends of 40-60% of total cementitious material are appropriate in most concrete mixture. On the other hand, slag cement blend containing less than 50% are recommended, when early strength is required or in the case of thin section construction during cold seasons [10]. The GGBS content and water to binder ratio were found as leading parameters influencing the long-term chloride diffusion in alkali activated slag concrete concretes [11]. Although high-volume slag cement blend concretes result in higher chloride penetration resistance and minimize steel corrosion, these concretes have low compressive strength and ease of deterioration under service load [12].

Nowadays, many researchers have broadly conducted research on the effect of concrete reinforcement corrosion and solve the chloride diffusion problem in concrete durability. One of the most effective ways to minimize chloride diffusion is to enhance concrete density. Sengul and Tasdemir [7] investigated the compressive strength and rapid chloride permeability of concrete cast from fly ash and GGBS. The results indicate that the chloride permeability of such concrete decreases significantly as the fineness of the slag cement increases, and that the compressive strength and chloride permeability are improved by the addition of pozzolans [7]. Particle size is a significant factor for facilitating a pozzolanic reaction in GGBS, and the strength development of concrete cast from slag cement increases with increasing particle fineness [13]. Cwirzen et al. [14] studied the effect of Baltic seawater on the frost durability of Portland cement concrete. The authors used sulfate-resistant Portland cement and a rapid-hardening Portland

cement combined with silica fume. Extensive surface scaling was detected on the silica fume concrete after exposure to 3% sodium chloride solutions. Further, Wu et al. [15] studied the combined effects of chloride attack and freeze-thaw action on silica fume concrete. The results indicate that the salt-scaling resistance of C50 concrete is superior to that of C30 concrete, and that the incorporation of 5% silica fume by mass of cementitious materials improves salt-scaling resistance. Moreover, Torii et al. [16] found that the chloride ion reacts with C_3A phase in the cementitious materials to produce the AFm phase $C_3A.CaCl_2.10H_2O$, or Friedel salt [16]. The existence of this compound in the cement matrix is believed to be significant for inhabiting the chloride-ion movement. Further, as the concrete strength class lessen, the resistance of concrete for freezing and thawing cycle also reduces. Peng et al. [17] indicates that the maximum chloride content appears around the exposure surface specifically in the loading points. In addition, Zhang et al. [18] also reported that after frequent exposure of freeze and thaw cycle weight loss in normal strength concrete becomes faster than that in high strength concrete.

Many scholars have studied the chloride ion diffusion of ordinary reinforced concrete under normal steady-state conditions [11, 12, 19-21]. In recent years, the effect of chloride ions with different environmental factors, such as sulphate attack, concrete stress, cracking, wet cycle, etc., has become the focus of attention. These studies are closer to the actual working environment of concrete structures used for coastal and offshore traffic projects, which are under coupling effect of freeze and thaw and, chloride exposure. However, the research on slag cement blend concrete durability in such environment is still in a very preliminary stage. This paper studied the coupling effect of chloride ion migration and freeze and thaw exposure as a function of the slag cement replacement ratio. The result of this study will widen the understanding of the effect of slag cement replacement on the chloride threshold level and its effect on chloride migration assessment under coupling effect of freeze and thaw and chloride exposure. Concrete specimens featuring various proportions of slag cement were produced and prepared to investigate their resistance to chloride ions and to determine the effects of a chloride ion attack and freeze–thaw cycles on concrete porosity and chloride ion threshold levels.

2. Experimental Details

2.1. Materials and mixture design

A standard Chinese Ordinary Portland Cement (OPC) (PO 42.5R and adhering to the ASTM International standard specification C989-09) [22] and a grade S-95 slag cement (with a compressive strength of 42.5 MPa) were chosen for this study and conformed to Chinese Standard Specifications GB175 and GB/T18046 [23]. The specific gravities of the OPC and slag cement were 3.15 and 2.89, respectively. River sand with a fineness modulus of 2.69 and a crushed granite coarse aggregate with a minimum size of 4.75 mm and maximum size of 10 mm were also used. The chemical compositions of the OPC and slag cement were characterized by x-ray fluorescence and are presented in Table 1.

The water-cementitious materials ratio selected for the experiment was 0.47, and the slag replacement percentages were 0% (control), 30%, 50%, and 70%. The proportions of the various concrete mixtures are presented in Table 2.

Table 1. Chemical composition of cement and GGBS (%wt.).

COMPONENT (%)	CEMENT	GGBS
SIO_2	17.945	26.713
AL_2O_3	4.465	14.748
FE_2O_3	3.558	0.472
CAO	64.562	43.093
MGO	3.751	10.145
RB_2O	0.005	0.000
NA_2O	0.178	0.380
K_2O	1.176	0.346
MNO	0.059	0.260
TIO_2	0.261	0.662
P_2O_5	0.064	0.010
NIO	0.005	0.003
ZNO	0.060	0.000
SPECIFIC GRAVITY	3.45	2.94

Table 2. Mix proportions of concrete per cubic meter.

MATERIALS	MIXTURE DESIGNATION			
	G-3	G-5	G-7	G-1
CEMENT (KG)	129.3	215.5	301.7	431
GGBS (KG)	301.7	215.5	129.3	-
WATER (KG)	202.7	201.7	202.7	202.7
W/C	0.47	0.47	0.47	0.47
COARSE AGGREGATES (KG)	1052.6	1052.6	1052.6	1052.6
FINE AGGREGATES (KG)	755.2	755.2	755.2	755.2

2.2. Specimens preparation and curing condition

The concretes were mixed using a revolving pan mixer with a capacity of 60 L. The components of each concrete mixture were batched by weight and the cement was then premixed with slag cement, sand, and coarse aggregates before the addition of water. Homogeneity was ensured by continuous mixing for approximately 5-6 min. Next, the cement was poured into cylindrical steel molds and compacted using a vibration table to form concrete specimens 400 mm in length and 100 mm in diameter (see Fig. 1). After 24 h, all specimens were demolded and cured in standard conditions of 20°C ± 2°C and 95% ± 2% relative humidity [24] for 28 d.

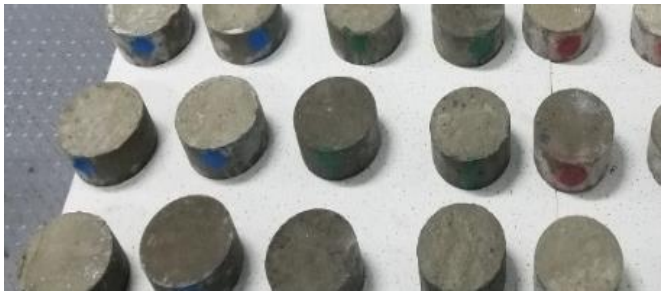

Fig. 1. Concrete samples cut from 400 mm length and 100Ø of concrete cylinder.

2.3. Test method

2.3.1. Freezing and thawing cycle tests

The freeze-thaw cycles were conducted in accordance with the ASTM International C666-15 "Standard Test Method for Resistance of Concrete to Rapid Freezing and Thawing" [25], and the machine utilized for this purpose is shown in Fig. 2. The thawing and freezing temperatures were set to 4°C and -16°C, respectively. However, the logged temperature data indicate that the measured high and low temperature ranges were 8°C ± 2°C and -17 ± 2°C, respectively (see Fig. 3). The concrete specimens were subjected to 4 h of freezing and 4 h of thawing to ensure completion of each process. After 5, 10, 15, 25, 40, and 50 freeze-thaw cycles, a sample 50 ± 2 mm in length was cut from each concrete specimen for a rapid chloride permeability test (RCPT), and the remainder of the specimen was subjected to further freeze-thaw cycles.

Fig. 2. Freezing and thawing machine.

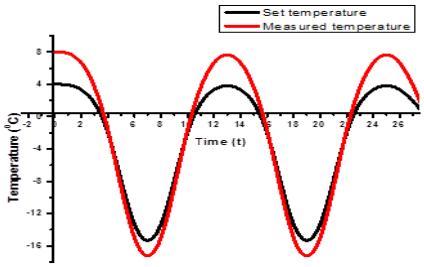

Fig. 3. Temperature control parameters of freeze-thaw cycle test.

2.3.2. Rapid chloride migration test

Eight samples were extracted from each concrete specimen for RCPTs after a curing period of 28 d and following the required number of freeze-thaw cycles [26]. A control group that was not subjected to freeze-thaw cycles and consisted of specimens from all concrete mixtures was also prepared for RCPTs. One day prior to testing, each specimen was saturated with limewater under vacuum conditions, as shown in Fig. 4. Vacuum suction was performed based on the procedures reported in [27-30]. Saturated-surface-dry concrete samples were placed inside the vacuum desiccator and a pressure of 10-50 mbar (1-5 kPa) was applied for 3 h.

Fig. 4. Vacuum suction desiccator machine.

While the vacuum pump was operating, the desiccator was slowly filled with limewater to completely immerse the samples, which were kept in the solution for approximately 24 h before air was allowed to re-enter the desiccator. On day 28, RCPTs were performed on the saturated samples according to the Chinese Standard Specification GB/T 50082-2009 and the ASTM International Test Specification C-1202 [29-31]. According to Lee et al. [32], the NT-Build 492 test method by Nordtest can be used to determine chloride migration coefficients under non-steady state conditions by harnessing an external voltage to drive the chloride ions into the concrete samples. Therefore, during the test, a power source with a voltage of 60 ± 0.05 V dc was used and the initial and final temperatures of the test solution were recorded. The durations of the RCPTs were determined based on the measured initial currents, as presented in Table 3, and the RCPT setup is shown in Fig. 5. A total of 56 cylindrical concrete samples were tested in batches of four. The catholyte solution was 10% NaCl by mass in distilled water (100 g of NaCl in 100 g of water, approximately 2 N) and the anolyte solution was 0.3 M of NaOH in distilled water (12 g of NaOH in 1 L of water). The ambient temperature was maintained at approximately 20°C-25°C [27]. The total volume of the solution in the catholyte reservoir was approximately 12 L, and approximately 300 mL of the anolyte solution was used as a liquid layer with a depth of at least 3 mm to cover the specimens.

Table 3. Duration (t) of the RCM test, based on the initial current (I_{30}) with 30V (mA)[27]**.**

I_{30} (MA)	DURATION T (HOUR)
<5	>96
5-10	48
10-15	24
15-20	24
20-30	24
30-40	24
40-60	24
60-90	24
90-120	8
>120	6

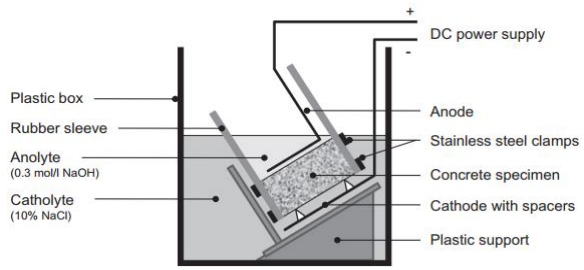

(a) Schematic RCPT measurement set-up according to NT-BUILD 492.

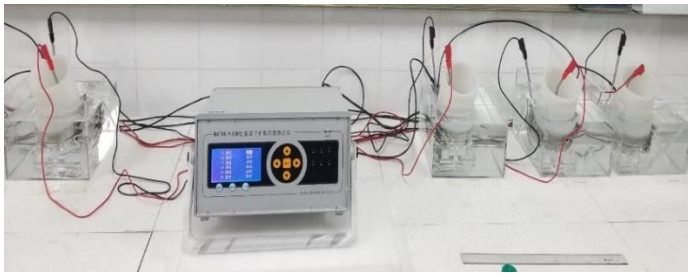

(b) NT-BUILD 492 Laboratory test setups.

Fig. 5. RCPT measurement set-up.

2.3.3. Measurement of chloride penetration depth

After RCPTs were conducted on the specimens (as illustrated in Figs. 6, 7 and 8), the penetration depths of the chloride ions were determined by spraying a 0.1 M $AgNO_3$ solution onto the concrete samples. Previous research has established that spraying silver nitrate solution onto fractured concrete can induce clear colour changes in both chloride-contaminated regions (which turn white) and chloride-free regions (which turn a brownish hue) [33-36]. This phenomenon is shown in Figs. 7 and 13, in which the observed depths of the white-coloured regions in the concrete samples are indicative of the depths of chloride penetration.

(a) Cutting of 50 mm sample for the RCP test.

(b) Axially splitting of concrete sample to determine the chloride depth penetration depth.

Fig. 6. Sample preparation.

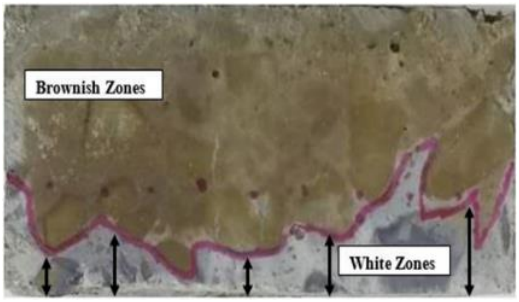

Fig. 7. Chloride penetration interface after spraying $AgNO_3$ solution indicator.

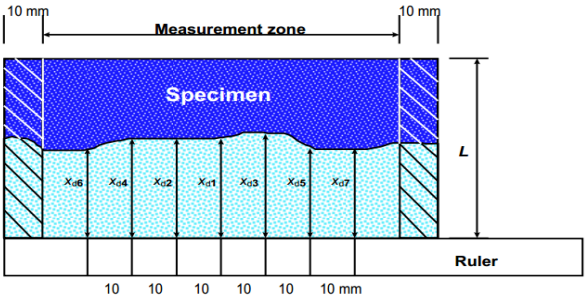

Fig. 8. Measurement of chloride penetration depth[27].

2.3.4. Chloride content test

After conducting RCPTs using a NELD-AL492, the water-soluble chloride ion contents of the samples were measured using a NELD-CL420 testing apparatus, which is shown in Fig. 9. These measurements required three stages: sample preparation, sample extraction, and analysis. After conducting RCPTs on measurement for 50 ± 2mm length and 100Ø of concrete samples, each sample was drilled along its surface to extract concrete that was ground in a mortar and passed through a 0.16 mm standard sieve to produce a powder [26, 37, 38]. The chloride ion contents of the samples were determined by following the procedure illustrated in Fig. 10 and utilizing the ion-selective electrodes (ISE) of the NELD-CL420 testing apparatus [38]. To avoid domination of the samples by aggregates, approximately equal quantities of cement paste were ensured for each sample. The chloride ion concentrations were determined using chloride-ion-sensitive electrodes and expressed as percentages of the weight of cement paste [39].

Fig. 9. NELD-CL420 chloride content measurement apparatus.

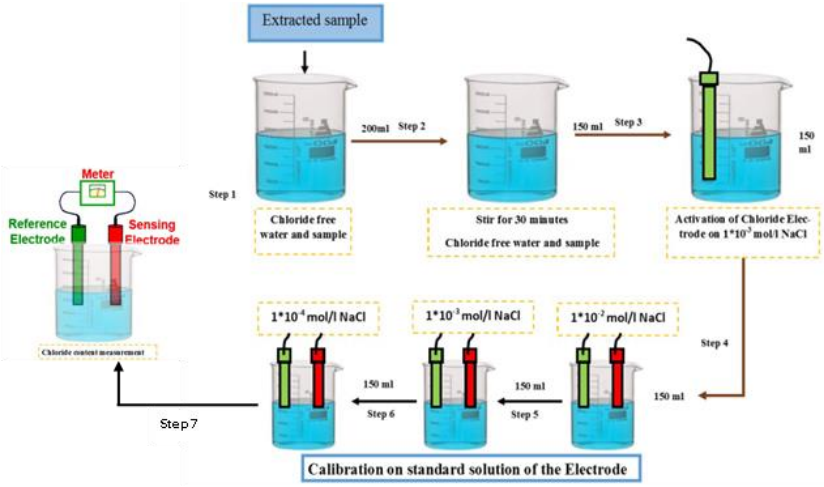

Fig. 10. Laboratory test set-up for water-soluble chloride content measurement[38, 40].

2.3.5. Mercury intrusion permeability test

Mercury intrusion porosimetry (MIP) instruments by Micromeritics were used to investigate the pore structures of the concrete samples in accordance with the ASTM International D4404-10 "Standard Test Method for Determination of Pore Volume and Pore Volume Distribution of Soil and Rock by Mercury Intrusion Porosimetry" [41]. An auto pore II 9220 mercury intrusion porosimeter with pressure range of 0.10~61000 psi was used to characterize the pore structure and determine the pore size diameter distribution of the GGBS blended concrete mixtures. The sample of 125mm^3 was extracted from the specimen's surface and then soaked under alcohol to terminate further hydration and then vacuum dried under 50°C for 48 h. The contact angel allowed for the MIP test was 130°.

3. Results and Discussion

3.1. Chloride migration coefficient

Capillary absorption, hydrostatic pressure, and diffusion are the possible means by which free chloride ions can penetrate the concrete structure. Most commonly the movement of chloride ion, under a concentration gradient happen to be due to diffusion. For this to happen, the concrete must have a persistent liquid phase and there must be a concentration gradient. Out of the three chloride-ion transport mechanisms outlined above that can affect the rebar inside the concrete structure by bring chlorides into the concrete is that of chloride ion diffusion. An experimental result in the determining chloride migration coefficient is presented in the following section.

After determining the test parameters from the RCPTs and measuring the chloride ion penetration depths, the chloride migration coefficients (D_{nssm},0) were calculated based on the following integrated form of the Nernst-Planck equation [27, 42]:

$$D_{nssm} = \frac{0.0239*(273+T)*L}{(U-2)*t} * \left(X_d - 0.0238\sqrt{\frac{(273+T)*L*X_d}{(U-2)}} * 10^{-12} \right) \quad (1)$$

In the above expression, (D_{nssm}, 0) denotes the non-steady state chloride ion migration coefficient (in m^2/s), U denotes the absolute value of the applied voltage (in V), T denotes the temperature (in °C as the average of the initial and final temperatures of the anolyte), L denotes the thickness of the specimen (in mm), X_d denotes the average chloride penetration depth of the specimen (in mm), and t denotes the test duration (in h) [42].

After completion of the RCPTs, the masses of the concrete specimens increased. Fig. 11 illustrates the mass variations of all concrete samples following RCPTs and exposure to various numbers of freeze-thaw cycles. The chloride ion penetration of the concrete specimens during the RCPTs resulted in the recorded increases in mass. These results agree with those of Liu et al. [36] who also confirmed an increase in concrete density following an RCPT due to chloride ion penetration [36]. Then, after obtaining the tested parameter from RCPT measurement, and the chloride penetration depth, the chloride migration coefficient (D_{RCM}) was calculated based on Eq. (1).

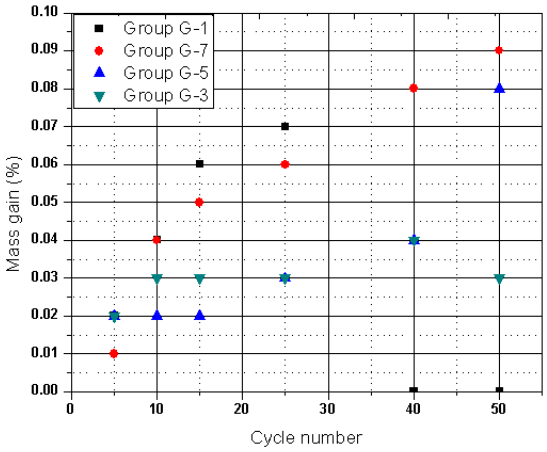

Fig. 11. Percentage of mass gain after RCM test and "n" number of freezing and thawing cycle exposure.

Figure 12 illustrates the variations in the chloride ion migration coefficients of the concrete specimens after exposure to various numbers of freeze-thaw cycles. These results demonstrate that mixtures containing higher percentages of replacement slag possessed lower chloride ion migration coefficients, and that the coefficients increased as the number of freeze-thaw cycles was increased. Groups G1 and G7 exhibited the most pronounced variations, whereas groups G5 and G3 performed comparatively well due to their lower cumulative pore volumes, as illustrated in Figs. 17 and 18.

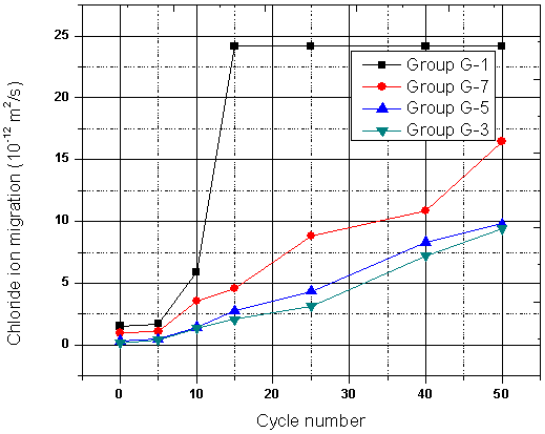

Fig. 12. Chloride migration coefficient Dnssm vs. Concrete mix group (Slag ratio for each concrete group is defined in Table. 2) after "n" number of freeze and thaw exposure

The rate of chlorides ingress into concrete structure mostly depends on the pore structure of the concrete, which is altered by many factors, cementitious materials, construction practices, and concrete age. The penetrability of concrete is explicitly related to the pore structure of the cement paste matrix. This will be influenced by the presence of supplementary cementing materials which provide pore structure development. The GGBS cement replacement ratio shows a significant effect on the cumulative pore volume of slag cement blended concrete, as the result shows in Fig. 17, the cumulative pore volume of G1 (100% OPC) and G7 (70% OPC), concrete group results a 41.5% and 25.3% increment compared to concrete group G3 (30% OPC). Whereas, replacing 50% cement by GGBS however results in 8.7% increments in cumulative pore volume after 5 freeze and thaw exposure, which underline the filling properties of GGBS cement. This is consistence with the previous research [11].

3.2. Effect of freeze-thaw cycle and resistance to chloride-ion penetration

Freezing and thawing damage is a concerning issue. The damage is significantly sped up, notably in bridge decks, marine concrete structures and roads, with associated action of de-icing salts, usually following in severe scaling at the surface. It has been well-known for years that freeze-thaw action in the temperate regions of the world can result extreme deterioration of concrete. Experimental works in determining the combined effect of freeze-thaw and chloride ion exposure is presented in the following section.

Figure 13 shows images of concrete specimens after exposure to various numbers of freeze-thaw cycles and subsequent RCPTs. The results presented in Fig. 12 prove that higher percentages of slag cement resulted in lower chloride ion migration coefficients. Further, concrete groups with relatively higher percentages of slag cement exhibited superior resistance to chloride ion penetration following exposure to freeze-thaw cycles [43, 44]. Therefore, it can be inferred that concrete produced without the addition of slag cement would exhibit relatively weaker

resistance to chloride ion penetration. According to the ASTM International Standard Test Method 1202-05, concretes containing slag cement and fly ash possess lower chloride ion permeabilities [45]. Additionally, Lee et al. [32] and Özbay et al. [46] have confirmed that concrete produced entirely from slag cement exhibits comparatively higher resistance to chloride ion penetration [32, 46].

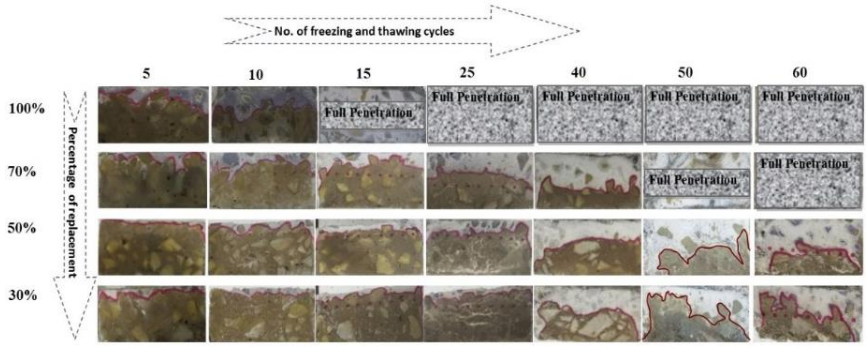

Fig. 13. Concrete specimens after the freezing and thawing and chloride ion penetration test.

Figure 13 shows the typical chloride ion penetration depths for all groups after exposure to various numbers of freeze-thaw cycles. As shown in Fig. 14, the average penetration depths for groups G1, G7, G5, and G3 prior to freeze-thaw exposure were 3.8, 2.7, 1.2, and 0.8 mm, respectively. Furthermore, chloride ion penetration depths increased for all groups as the number of freeze-thaw cycles was increased. For instance, the average chloride penetration depths for concrete groups G1, G7, G5, and G3 after five freeze-thaw cycles were 4.5, 3.1, 1.59, and 1.5 mm, respectively. After 15 cycles, the chloride ions had fully penetrated the concrete sample cast from 100% OPC (G1), whereas group G7 was fully penetrated by chloride ions after 50 cycles. The remaining groups (G5 and G3) experienced full-scale penetration after 60 cycles (see Fig. 13). These results confirm that the extent of chloride ion penetration was dependent on the permeability of the concrete specimens in addition to other factors [44]. Finally, MIP tests revealed that the porosity of group G7 increased as the number of freeze-thaw cycles was increased.

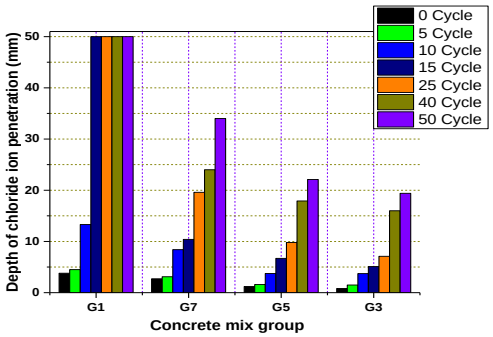

Fig. 14. Effect of freeze and thaw on chloride ion penetration depth tested by RCPT.

3.3. Concentration of water-soluble Chloride ion

The chloride ion migration coefficients of all four groups were measured after each freeze–thaw cycle. The concentrations of water-soluble chloride ions in mol/L and as percentages were determined and are presented in Fig. 15. These results indicate that both the slag content of the concrete samples and the number of freeze–thaw cycles affected the concentrations of water-soluble chloride ions. The free chloride migration coefficient of the concrete mixture composed of 70% slag cement (G3) was substantially lower than those of the other groups. Further, Özbay et al. [46] reported that an increase in slag content from 55% to 81% in engineered cementitious composite mixtures resulted in a decrease in the total volume of voids, porosity, and water absorption [46]. Moreover, concrete mixtures containing 100% OPC (G1), 30% slag (G7), 50% slag (G5), and 70% slag (G3) exhibited percentage increases in chloride ion concentration of 0.62%, 0.065%, 0.0625%, and 0.0025%, after 25 cycles respectively. Hence, these results clearly show that increasing the percentage of slag cement caused a decrease in the chloride ion migration coefficients [47].

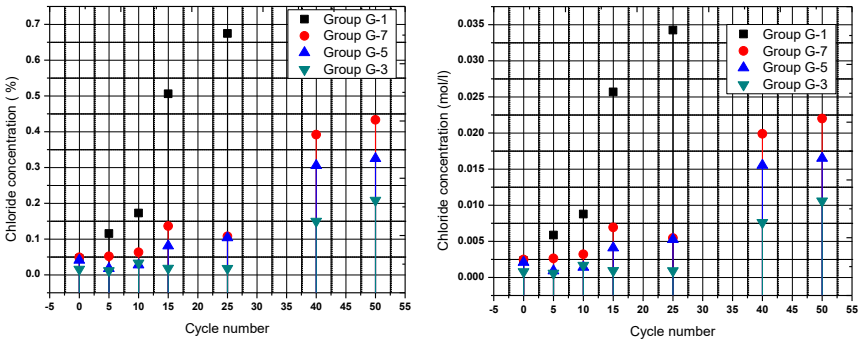

(a) Chloride concentration in Percentage. **(b) Chloride concentration in mol/l.**

Fig. 15. Chloride concentration under different freezing and thawing exposure.

Based on these experimental results and those reported in by Neville and Brooks [13] and Ann and Song [39], the incorporation of GGBS into cement is an effective method of reducing chloride ion penetration relative to OPC [21]. The chloride ions react with the C_3A phase in the cementitious materials to produce the AFm phase $C_3A{\cdot}CaCl_2{\cdot}10H_2O$, also known as Friedel's salt [16]. The presence of Friedel's salt in the cement matrix inhibits chloride ion migration.

Papadakis G. [48] experimentally shows the effect of supplementary cementing materials on concrete resistance against chloride ingress, the experimental result proves that concrete groups incorporating SCM exhibit significantly lower chloride content compared to control concrete group with OPC, when exposed to chloride. Further, Torii et al. [16], and his colleges reveals that, the RCPT result for concrete with SCM shows less permeability to chloride ions than OPC under same exposure condition. Similarly, Kopecskó and Balázs [21] also reported that, with increase in slag content of cement the chloride migration coefficients and chloride penetration depth decrease as well.

3.4. Mercury intrusion permeability analysis (MIP)

Figures 17 and 18 present the MIP test results for all concrete groups after exposure to freeze–thaw cycles. The average pore diameters of groups G1, G7, G5, and G3 after five cycles were 11.25, 26.68, 15.40, and 10.86 nm, respectively. Furthermore, specimens with relatively higher percentages of slag cement exhibited relatively lower internal porosities; the internal porosities for groups G1, G7, G5, and G3 were 14.4%, 12.09%, 10.2%, and 9.4%, respectively, as it is computed from the MIP results. As shown in Fig. 16, group G1 possessed the highest measured pore volume, and porosity decreased with the increasing percentage of slag replacement. Therefore, the MIP test results verify that, as the slag replacement ratio increased, the porosity and integral pore distribution of the concrete decreased significantly [49].

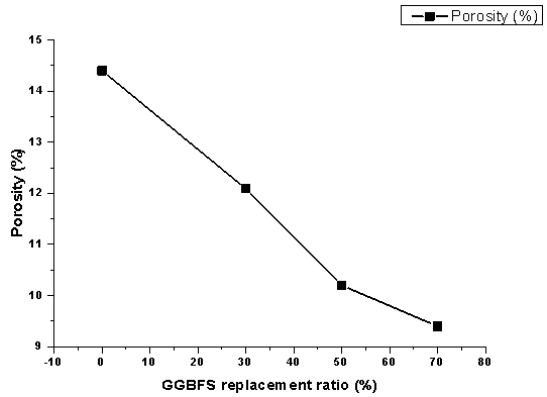

Fig. 16. Total porosities of the specimens as a function of GGBFS replacement ratio.

Previous papers have reported that the total pore volume of slag concrete is smaller than that of conventional concrete [50, 51]. For example, Bouikni et al. [52] utilized MIP tests to study the effects of various slag replacement ratios on pore-size distributions, and the results proved that concrete incorporating slag cement exhibited significantly more compacted pore structures than OPC concrete. Figures 17 and 18 show the pore-size diameter distributions of the tested concrete specimens. To characterize these distributions, the pore diameters were divided into three classes: macropores (>100 nm), mesopores (50-100 nm and 3-50 nm), and micropores (<3 nm) [45]. Mesopores accounted for 70%-90% of the total pore volumes in all specimens [49].

Figure 17 shows the MIP results for the cumulative pore volumes in the concrete specimens after five freeze-thaw cycles. Group G1 exhibited a loose structure that exacerbated chloride ion penetration, and group G7 exhibited similar properties after 50 cycles. Groups G5 and G3 exhibited more compact pore structures and performed comparatively better following the chloride ion permeability test and exposure to the freeze-thaw cycles.

In particular, the average pore diameters of group G7 after 5, 10, and 15 freeze-thaw cycles were 26.68, 16.36, and 17.94 nm, respectively. Furthermore, the internal porosity of group G7 after 5, 10, and 15 freeze-thaw cycles were 12.09%, 12.9%, and 12.9%, respectively. The MIP test results revealed that the porosities

of all concrete specimens increased with the increasing number of freeze-thaw cycles, and that the porosity of group G7 increased by 0.81% between 5 and 15 freeze–thaw cycles. Moreover, Cheng et al. [50] demonstrated that, as the slag replacement ratio is increased, the capillary pore volume decreases.

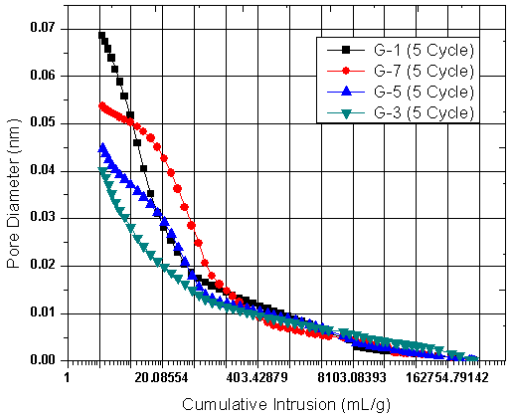

Fig. 17. Comparison between cumulative intrusion and pore size diameter of concrete specimens after 5 freeze-thaw cycles.

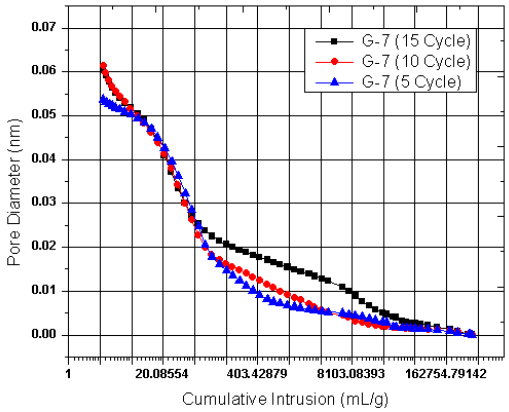

Fig. 18. Variation in cumulative intrusion with pore size diameter during 5,10 and 15 freeze-thaw cycles.

4. Conclusion

Concretes produced with GGBS and cured in standard conditions were exposed to varying numbers of freeze-thaw cycles and a chloride ion attack. Concrete specimens made from pure OPC (PO 42.5R) were also exposed to the same conditions. The chloride ion threshold levels, migration coefficients, and penetration depths were investigated in addition to the porosities of the concrete samples. The porosities and pore-size distributions were determined via MIP tests. Furthermore, the chloride ion threshold levels and migration coefficients were analysed using NELD-CL420 ISEs and a NELD-AL492 RCPT apparatus, respectively. The following conclusions are drawn from the obtained test results:

- Repeated exposure to freeze-thaw cycles increased the pore volumes of samples that contained a percentage of slag replacement, and this trend was enhanced in the control group that contained 0% slag. However, even after exposure to freeze-thaw cycles, concrete samples containing slag cement exhibited more compacted pore structures than that of the OPC concrete. These changes in the internal pore structures were evident in the demonstrated resistances to chloride ion penetration.
- Due to their superior chloride-binding capacities, the chloride ion migration coefficients of the slag-blended cements were lower than that of the OPC.
- Concrete specimens with higher percentages of slag exhibited greater chloride-binding capacities. Specifically, groups G1, G7, G5, and G3 exhibited chloride ion increases of 0.62%, 0.065%, 0.0625%, and 0.0025%, after 25 cycles respectively. Further, the chloride ion migration coefficients decreased as the slag replacement ratio was increased. Moreover, the concrete with a slag replacement ratio of 70% (group G3) was verified as possessing a relatively higher resistance to the freeze-thaw cycles.
- Chloride ion penetration depths decreased as the percentage of slag replacement increased but increased in all specimens with exposure to increasing numbers of freeze-thaw cycles.

Declarations

Conflict of interest

The authors declare that they have no conflict of interest.

Availability of data and materials

The research data used to support the finding of this study are described and included in the article. Furthermore, some of the data used in this study is also supported by providing references as described in the article.

Authors' contributions

All authors contributed substantially to all aspects of this article. All authors read and approved the final manuscript.

References

1. Andrew, R.M. (2018). Global CO_2 emissions from cement production. *Earth Science Data*, 10, 195-217.
2. Siddique, R.; and Kaur, D. (2012). Properties of concrete containing ground granulated blast furnace slag (GGBFS) at elevated temperatures, *Journal of Advanced Research*, 3(1), 45-51
3. Shumuye, E.D.; and Jun, Z. (2018). A review on ground granulated blast slag (GGBS) in concrete. *Proceeding of the 8th International Conference on Advances in Civil and Structural Engineering*. Kuala Lumpur, Malaysia. 5-10.
4. Chen, E.Y. (2006). Application of GGBS in China -A gradual shift from cost-savings to durability. *Proceeding of the Second Global Slag Conference and Exhibition*. Bangkok, Thailand, 1-10

5. Maholtra, V.M. (1989). Fly ash, slag, silica fume, and natural pozzolans in concrete. *Proceedings of the Third International Conference on Fly Ash, Silica Fume, Slag and Pozzolans in Concrete*. Trondheim, Norway.
6. Koh, K.T.; Park, C.J.; Ryu, G.S.; Park, J.J.; Kim, D.G.; and Lee, J.H. (2013). An experimental investigation on minimum compressive strength of early age concrete to prevent frost damage for nuclear power plant structures in cold climates. *Nuclear Engineering and Technology*, 45(3), 393-400.
7. Sengul, O.; and Tasdemir, M.A. (2009). Compressive strength and rapid chloride permeability of concretes with ground fly ash and slag. *Journal of Materials in Civil Engineering*, 21(9), 494-501.
8. Holthuizen, P.E.; Çopuroğlu, O.; and Polder, R.B. (2018). *High tech concrete: Where technology and engineering meet*. Chapter: Chloride ingress of carbonated blast furnace slag cement mortars. Dordrecht: Springer International Publishing, 73–82.
9. Dhir, R.K.; El-Mohr, M.A.K.; and Dyer, T.D. (1997). Developing chloride resisting concrete using PFA. *Cement and Concrete Research*, 27(11), 1633-1639.
10. ACI Committee 233R-03 (2000). Ground granulated blast-furnace slag as a cementitious constituent in concrete. *Material Journal*, 92(3), 321-322.
11. Zhang, J.; Ma, Y.; Zheng, J.; Hu, J.; Fu, J.; Zhang, Z.; Wang, H. (2020). Chloride diffusion in alkali-activated fly ash/slag concretes: Role of slag content, water/binder ratio, alkali content and sand-aggregate ratio, *Construction and Building Materials*, 261, 1-12.
12. Cheewaket, T.; Jaturapitakkul, C.; and Chalee, W. (2014). Concrete durability presented by acceptable chloride level and chloride diffusion coefficient in concrete: 10-year results in marine site. *Materials and Structures*, 47(9), 1501-1511.
13. Neville, A.M.; and Brooks, J.J. (2010). *Concrete Technology* (2nd ed.). Canada: Pearson Education.
14. Cwirzen, A.; Sztermen, P.; and Habermehl-Cwirzen, K. (2014). Effect of Baltic seawater and binder type on frost durability of concrete. *Journal of Materials in Civil Engineering*, 26(2), 283-287.
15. Wu, Z.; Shi, C.; Gao, P.; Wang, D.; and Cao, Z. (2015). Effects of deicing salts on the scaling resistance of concrete. *Journal of Materials in Civil Engineering*, 27(5), 04014160.
16. Torii, K.; Sasatani, T.; and Kawamura, M. (1997). Application of rapid chloride permeability test to evaluate the chloride-ion penetration into concrete. *ACI Symposium Paper*, 170, 421-436.
17. Peng, L.; Zhao, Y.; and Zhang, H. (2021). Flexural behavior and durability properties of recycled aggregate concrete (RAC) beams subjected to long-term loading and chloride attacks. *Construction and Building Materials*, 277, 1-14.
18. Zhang, X.; Wang, L.; and Zhang, J. (2017). Mechanical behavior and chloride penetration of high strength concrete under freeze-thaw attack. *Cold Regions Science and Technology*, 142, 17–24.
19. Zhang, P.; and Li, Q.F. (2013). Effect of polypropylene fiber on durability of concrete composite containing fly ash and silica fume. *Composites Part B: Engineering*, 45(1), 1587-1594.

20. Al-Sodani, K.A.A.; Al-Zahrani, M.M.; Maslehuddin, M.; Al-Amoudi, O.S.B.; and Al-Dulaijan, S.U. (2021). Chloride diffusion models for Type I and fly ash cement concrete exposed to field and laboratory conditions. *Marine Structures*, 76, 1-14.
21. Kopecskó, K.; and Balázs, G.L. (2017). Concrete with improved chloride binding and chloride resistivity by blended cements. *Advances in Materials Science and Engineering*, 2017, 1-13.
22. ASTM Committee (2004). *Standard specification for ground granulated blast-furnace slag for use in concrete and mortars (ASTM C989-06).* American Society for Testing and Material, Pennsylvania, United State of America.
23. China Building Materials Science Research Institute. (2007). *Moderate-heat portland cement, low-heat portland cement (GB 175-2007).* Standardization Administration of the People's Republic of China, China.
24. ASTM Committee. (2004). *Standard practice for making and curing concrete test specimens in the laboratory (ASTM C192M-07)*. American Society for Testing and Material, Pennsylvania, United State of America.
25. ASTM Committee. (2004). *Test method for resistance of concrete to rapid freezing and thawing (ASTM C666M-15).* American Society for Testing and Material, Pennsylvania, United State of America .
26. Nordtest Method (1995). *Concrete, hardened: Accelerated chloride penetration (NT Build 443)*. Finland: Nordtest.
27. EU-Project CHLORTEST (2005). *Guideline for practical use of methods for testing the resistance of concrete to chloride ingress (G6RD-CT2002-00855)*. SP Swedish National Testing and Research Institute, Sweden.
28. Spiesz, P.; and Brouwers, H.J.H. (2012). Influence of the applied voltage on the rapid chloride migration (RCM) test. *Cement and Concrete Research*, 42(8), 1072-1082.
29. Ministry of Housing and Urban-Rural Construction of the People's Republic of China. (2010). *Standard for test method of long-term performance and durability of ordinary concrete (GB/T 50082-2009)*. Standardization Administration of the People's Republic of China, China.
30. RCM-NTB. (2005). RCM-NTB Service and operation manual. Retrieved January 3, 2010, from https://www.redlinestands.com/manuals/NTB550_Manual.pdf
31. ASTM Committee (2010). *Test method for electrical indication of concrete's ability to resist chloride ion penetration (ASTM C1202-10).* American Society for Testing and Material, Pennsylvania, United State of America.
32. Lee, B.; Kim, G.; Nam, J.; Cho, B.; Hama, Y.; and Kim, R. (2016). Compressive strength, resistance to chloride-ion penetration and freezing/thawing of slag-replaced concrete and cementless slag concrete containing desulfurization slag activator. *Construction and Building Materials*, 128, 341-348.
33. Noushini, A.; Castel, A.; Aldred, J.; and Rawal, A. (2019). Chloride diffusion resistance and chloride binding capacity of fly ash-based geopolymer concrete. *Cement and Concrete Composites*, 105, 1-19.
34. Hasholt, M.T.; and Jensen, O.M. (2015). Chloride migration in concrete with superabsorbent polymers. *Cement and Concrete Composites*, 55, 290-297.

35. Dong, B.; Wu, Y.; Teng, X.; Zhuang, Z.; Gu, Z.; Zhang, J.; Xing, F.; and Hong, S. (2019). Investigation of the Cl- migration behavior of cement materials blended with fly ash or/and slag via the electrochemical impedance spectroscopy method. *Construction and Building Materials*, 211, 261-270.
36. Liu, J.; Wang, X.; Qiu, Q.; Ou, G.; and Xing, F. (2017). Understanding the effect of curing age on the chloride resistance of fly ash blended concrete by rapid chloride migration test. *Materials Chemistry and Physics*, 196, 315-323.
37. RILEM TC 178-TMC. (2002). Recommendation of RILEM TC 178-TMC: 'Testing and modelling chloride penetration in concrete' Analysis of total chloride content in concrete. *Materials and Structures*, 35(253), 583–585.
38. NELD-CL420. (2005). NELD-CL420 Service and operation manual v1.pdf, Beijing NEL Limited
39. Ann, K.Y.; Song, H.W. (2007). Chloride threshold level for corrosion of steel in concrete. *Corrosion Science*, 49(11), 4113-4133.
40. ASTM Committee (2016). *Standard test method for determining the apparent chloride diffusion coefficient of cementitious mixtures by bulk diffusion (ASTM C1556)*. American Society for Testing and Material, Pennsylvania, United State of America.
41. ASTM Committee (2018). *Standard test method for determination of pore volume and pore volume distribution of soil and rock by mercury intrusion porosimetry (ASTM D4404-18)*. American Society for Testing and Material, Pennsylvania, United State of America.
42. Hasholt, M.T.; and Jensen, O.M. (2015). Chloride migration in concrete with superabsorbent polymers. *Cement and Concrete Composites*, 55, 290-297.
43. Jariyathitipong, P. (2014). *Improving the durability of concrete through the use of ground granulated blast furnace slag and blast furnace slag sand.* Doctoral dissertation, Okayama University, Japan.
44. Yuksel, I. (2018). *Waste and supplementary cementitious materials in concrete*. Chapter: Blast-furnace slag. Elsevier, 361-415.
45. ASTM Committee (2010). *Standard test method for electrical indication of concrete's ability to resist chloride ion penetration (ASTM C1202-10).* American Society for Testing and Material, Pennsylvania, United State of America.
46. Özbay, E.; Karahan, O.; Lachemi, M.; Hossain, K.M.A.; and Atis, C.D. (2013). Dual effectiveness of freezing-thawing and sulfate attack on high-volume slag-incorporated ECC. *Composites Part B: Engineering*, 45(1), 1384-1390.
47. Orosz, K. (2017). *Early age autogenous deformation and cracking of cementitious materials - implications on strengthening of concrete structures.* Doctoral dissertation, Luleå University of Technology.
48. Papadakis, V.G. (2000). Effect of supplementary cementing materials on concrete resistance against carbonation and chloride ingress. *Cement and Concrete Research*, 30(2), 291-299.
49. Choi, Y.C.; Kim, J.; and Choi, S. (2017). Mercury intrusion porosimetry characterization of micropore structures of high-strength cement pastes incorporating high volume ground granulated blast-furnace slag. *Construction and Building Materials*, 137, 96-103.

50. Cheng, A.S.; Yen, T.; Liu, Y.W.; and Sheen, Y.N. (2008). Relation between porosity and compressive strength of slag concrete. *Proceeding of the 2008 Structures Congress.* Vancouver, British Columbia, Canada, 1-8.
51. Kim, T.; Kim, I.T.; Seo, K.Y.; Park, H.J. (2019). Strength and pore characteristics of OPC-slag cement paste mixed with polyaluminum chloride. *Construction and Building Materials*, 223, 616-628.
52. Bouikni, A.; Swamy, R.N.; and Bali, A. (2009). Durability properties of concrete containing 50% and 65% slag. *Construction and Building Materials*, 23(8), 2836-2845.
53. Lawrence, M.; and Jiang, Y. (2017). *Bio-aggregates based building materials.* Chapter: Porosity, pore size distribution, micro-structure. Dordrecht: Springer Netherlands, 39-71.